Research in Astronomy and Astrophysics, 24:035020 (17pp), 2024 March https://doi.org/10.1088/1674-4527/ad256e
© 2024. National Astronomical Observatories, CAS and IOP Publishing Ltd. Printed in China and the U.K.

A Quick Calculation Method for Radiation Pattern of Submillimeter Telescope with Deformation and Displacement

Jia You, Yi-Wei Yao, and Zheng Wang
School of Automation, Southeast University, Nanjing 210096, China; wangz@seu.edu.cn
Received 2023 November 16; revised 2024 January 27; accepted 2024 February 1; published 2024 March 6

Abstract

Radiation pattern captures the electromagnetic performance of reflector antennas, which is significantly affected by the deformation of the primary reflector due to gravity and the displacement of the secondary reflector. During the design process of large reflector antennas, a substantial amount of time is often dedicated to iteratively adjusting structural parameters and validating electromagnetic performance. To improve the efficiency of the design process, we first propose an approximate calculation method of optical path difference (OPD) for the deformation of the primary reflector under gravity and the displacement of the secondary reflector. Then an OPD fitting function based on the modified Zernike polynomials is proposed to capture the phase difference of radiation over the aperture plane, based on which the radiation pattern will be obtained quickly by the aperture field integration method. Numerical experiments demonstrate the effectiveness of the proposed quick calculation method for analyzing the radiation pattern of a 10.4 m submillimeter telescope antenna at its highest operating frequency of 856 GHz. In comparison with the numerical simulation method based on GRASP (which is an antenna electromagnetic analysis tool combining physical optics (PO) and physical theory of diffraction (PTD)), the quick calculation method reduces the time for radiation pattern analysis from more than one hour to less than two minutes. Furthermore, the quick calculation method exhibits excellent accuracy for the figure of merit (FOM) of the radiation pattern. Therefore, the proposed quick calculation method can obtain the radiation pattern with high speed and accuracy. Compared to the time-consuming numerical simulation method (PO and PTD), it can be employed for quick analysis of the radiation pattern for the lateral displacement of the secondary reflector and the deformation of the primary reflector under gravity in the design process of a reflector antenna.

Key words: instrumentation: high angular resolution – methods: data analysis – methods: analytical

1. Introduction

Large reflector antennas have a wide range of applications in space exploration and radio astronomy, and they provide high gain, high angular resolution and narrow beam (Rahmat-Samii & Haupt 2015). Typically, the design process of a large reflector antenna involves several stages, including conceptual design, optimized structural design and final design (Baars & Kärcher 2018), all of which aim at achieving a specific figure of merit (FOM). During the conceptual design stage, initial design parameters are established, and a suitable design scheme is determined. Subsequently, in the optimized structural design stage, the FOM of the reflector antenna is rigorously examined and enhanced. Finally, in the last detailed design stage, comprehensive verification is conducted on all subsystems to ensure compliance with the specified FOM.

For large reflector antennas working at high frequencies, the optimized structural design stage is usually very time-consuming due to repeated performance verification experiments under various operating conditions. One crucial FOM that requires verification during this stage is the pointing accuracy, which is primarily influenced by gravity load. In general, the pointing accuracy must be within 10% of the antenna's half-power beamwidth (HPBW; Safak 1990). The FOM of the radiation pattern (i.e., the pointing of the main lobe (POML), the HPBW and the side lobe level (SLL)) serve as crucial indicators for measuring the pointing accuracy. The radiation pattern can be obtained through a combination of finite element analysis (FEA) and numerical simulation (Feng et al. 2019) in the optimized structural design stage. However, obtaining the radiation pattern by using numerical simulation tools for large-diameter and high-frequency reflector antennas typically requires a significant amount of time. For example, it may take more than an hour to obtain the radiation pattern for a 10.4 m antenna of a submillimeter telescope working at a high frequency of over 800 GHz by simulation with GRASP (an often-used radiation pattern analysis tool).

Pointing accuracy is significantly affected by the deformation of the primary reflector due to gravitational load and the displacement of the secondary reflector. Therefore, efficiently calculating the radiation pattern considering the deformation and displacement of the reflector can significantly reduce the

time for evaluating pointing accuracy during the optimized structural design phase. Improvement in efficiency enhances the overall antenna design process. In recent years, fast and accurate calculation of the radiation pattern for deformed and displaced reflectors has become an increasingly important research topic.

For the calculation of the far-field radiation pattern of a reflector antenna, several numerical methods such as physical optics (PO) and the physical theory of diffraction (PTD) are widely used (McNamara et al. 1990). To determine the gain and aperture efficiency of a reflector antenna operating in the frequency range of 1.28–1.75 GHz, Du et al. (2016) employed GRASP-10 to compute radiation patterns, which is a numerical tool that utilizes PO and PTD for radiation pattern analysis. Although numerical tools like GRASP-10 are precise in determining the radiation pattern of reflector antennas, their computational complexity may result in considerable time consumption, particularly for large reflector antennas and high frequency ranges. Since the sidelobes away from the main lobe region are much less significant compared to those close to the main lobe region, only a limited range of angle needs to be considered when analyzing the radiation pattern numerically. In this way, the time for radiation pattern analysis can be shortened.

Duan & Wang (2009) simultaneously considered systematic error and random error of the primary reflector antenna by combining the Ruze formula and the mechanical-electromagnetic-field coupling model (MEFCM), and calculated the pointing error and gain loss under gravitational load and wind force. A key procedure in the MEFCM is the derivation of the aperture field optical path difference (OPD), especially for dual reflector antennas. Xiang et al. (2019) investigated the effect of the secondary reflectors displacement on the OPD by decomposing the secondary reflector parameters using an MEFCM to represent the actual far-field beam pattern as a synthesis of the ideal and error beams, and developed a new method based on parameter iteration techniques to determine the optimal secondary reflector position for Cassegrain antennas to improve the electromagnetic performance subject to gravitational distortion.

The deformation distribution over the reflector surface also affects the radiation pattern (Lian et al. 2015). Li et al. (2012) employed the finite element (FE) method to perform a thermal structural analysis, obtain the temperature distribution of the entire antenna and calculate the electromagnetic characteristics of the antenna using the far-field pattern formula. The study showed that the degradation of the electromagnetic characteristics depends not only on the surface root mean square error (RMSE) but also on the deformation distribution, particularly for the pointing error and the SLL. The temperature distribution of the antenna is hard to obtain, and it takes a long time for the FE simulation tool to carry out FE modeling and post-processing. To address these limitations, Zhang et al. (2023) presented a surrogate model based on extreme gradient boosting (XGBoost) and deep convolutional neural networks (CNN) to get the deformation distribution of the primary reflector quickly. Fu et al. (2022) considered the displacement of the secondary reflector under gravitational load, and proposed a measurement method for the deformation distribution of the primary reflector and the displacement of the secondary reflector for a 70 m antenna at different zenith angles (ZAs) by laser scanner.

The research mentioned above provides evidence that the magnitude and distribution of the primary reflectors deformation and the displacement of the secondary reflector will significantly affect the electromagnetic performance of the reflector antenna. Therefore, this paper aims to propose a quick calculation method for evaluating the radiation pattern of large-diameter reflector antennas working in high frequency bands affected by the deformation of the primary reflector under gravitational load and the displacement of the secondary reflector. First, the deformation distribution of the primary reflector under gravitational load is obtained by FEA at different ZAs. Then we propose an approximate OPD calculation method based on the displacement of the secondary reflector and the best-fit paraboloid (BFP) of the primary reflector. Finally, a mathematical formulation based on the modified Zernike polynomials is proposed to fit the calculated OPD, and then the radiation pattern and its FOMs can be obtained by the aperture field integration method (AFIM). The calculated radiation patterns and their FOMs are compared with those obtained by simulation with GRASP (which is an antenna electromagnetic analysis tool combining PO and PTD). Experimental results show that for large-diameter reflector antennas working at high frequencies, the proposed quick calculation method can not only significantly reduce the calculation time but also achieve high accuracy compared to the simulation method.

The remainder of this paper is organized as follows: Section 2 describes the methodology for quickly calculating radiation patterns and the method for verifying their validity. In Section 3, the quick calculation method of the radiation pattern is presented. Section 4 gives the design of the dual reflector model in GRASP. In Section 5, numerical experiments are conducted to verify the rapidity and accuracy of the proposed quick calculation method by comparing it with the results obtained by simulation with GRASP. Section 6 concludes the paper and presents some issues for future research.

2. Methodology

The gravitational load can induce the deformation of the primary reflector in submillimeter telescopes. Electromagnetic simulation software, such as High Frequency Structure Simulator (HFSS), and antenna design software, such as GRASP, can be employed to simulate the radiation pattern of

antennas. However, for a submillimeter telescope with a large aperture diameter and working at high frequencies, such as the Caltech Submillimeter Observatory (CSO) telescope with a diameter of 10.4 m, the range of observed radiation wavelengths typically falls between 2 mm and 350 μm, and its highest working frequency is 856 GHz.[1] Increasing the ratio of the antenna size to wavelength will increase the time consumed for obtaining the radiation pattern by simulation. As radiation pattern analysis plays an important role in determining the pointing accuracy, a rapid method of analyzing radiation patterns can significantly reduce the time required for verifying the pointing accuracy during the structural design phase for large-diameter reflector antennas working at high frequencies.

In this paper, we investigate the impact of the deformation of the primary reflector and the displacement of the secondary reflector on the radiation pattern of a submillimeter telescope and the quick calculation method of the radiation pattern. The schematic overview of the research methodology is depicted in Figure 1, which can be explained as below and in which Steps 1–3 are conducted in Ansys, Steps 4–5 are conducted in GRASP and Steps 6–8 are the procedure of a quick calculation method of radiation pattern analysis:

In Ansys, the following three operations are performed:

1. Perform the FEA of the primary reflector by using Ansys to derive its initial deformation distribution, i.e., a group of data capturing the coordinates (in the ground coordinate system) of the nodes of the deformed primary reflector mode in Ansys.
2. Calculate the BFP of the deformed primary reflector by the least squares method.
3. Develop the reflector coordinate system based on the BFP parameters and obtain the deformation distribution of the primary reflector in the reflector coordinate system, i.e., a group of data capturing the coordinates (in the reflector coordinate system) of the nodes of the deformed primary reflector model in Ansys.

In GRASP, the following two processing steps are executed:

4. Export the deformation distribution data of the primary reflector in the reflector coordinate system from Ansys and import the data to GRASP.
5. Generate the antenna model of a submillimeter telescope according to the imported deformation distribution data of the primary reflector, the focal length of the BFP and the displacement of the secondary reflector. Then conduct the radiation pattern analysis by numerical simulation.

Steps 6–8 are for quick calculation of the radiation pattern:

6. Calculate the OPD between the deformed and ideal primary reflectors in the reflector coordinate system.
7. Construct a mathematical formulation based on Zernike polynomial terms to fit the OPD arising from the deformation of the primary reflector and the displacement of the secondary reflector.
8. An AFIM is employed to compute the radiation pattern arising from the variation in optical path length.

The last two operations are comparative and improvement studies.

9. Conduct a comparison between the calculated radiation pattern and the simulated radiation pattern.
10. Modify the Zernike polynomial terms of the OPD fitting function according to the comparison result between simulation and calculation.

3. Quick Calculation Method for Radiation Pattern

In this section, the main procedures for quickly calculating the radiation pattern are described.

3.1. The Best-fit Paraboloid

The structural FEA of the primary reflector model is performed by using an FE solver in Ansys subject to gravitational load at different ZAs. The CSO telescope is taken as an example to illustrate and verify the proposed method, and the FE model of the CSO telescope is constructed based on the structural parameters provided by Woody et al. (1994). Figure 2 presents the FE model of the CSO telescope in the ground coordinate system (i.e., the $X_0Y_0Z_0$-coordinate system, where the positive direction of the X_0-axis is perpendicular to the Y_0Z_0 plane and pointing to the readers) at ZA = 45°, which shows a detailed description of the primary reflector, the direction of gravity, the zenith direction and ZA of the primary reflector. Gravity points to the negative direction of the Z_0-axis, the zenith direction points to the positive direction of the Z_0-axis, and the primary reflector rotates around the elevation axis during observation, which is perpendicular to the zenith direction and the direction of the optical axis of the primary reflector. In addition, the angle between the direction of the optical axis of the primary reflector and the zenith direction is the ZA. In order to describe the deformation distribution of the primary reflector under different ZAs clearly, the antenna coordinate system (i.e., the *XYZ*-coordinate system) is constructed (also see Figure 2), in which the origin is the vertex of the primary reflector, the *Z*-axis is the optical axis of the primary reflector, the *X*-axis is parallel to the elevation axis and pointing to the readers, and the *Y*-axis is perpendicular to the *Z*-axis and the *X*-axis. Figure 3 shows the deformation distribution of the primary reflector at ZA = 45° under gravitational load along the *X*-axis, *Y*-axis and *Z*-axis respectively in the *XYZ*-coordinate system, as well as the total deformation distribution.

[1] http://www.cso.caltech.edu/wiki/cso/science/overview

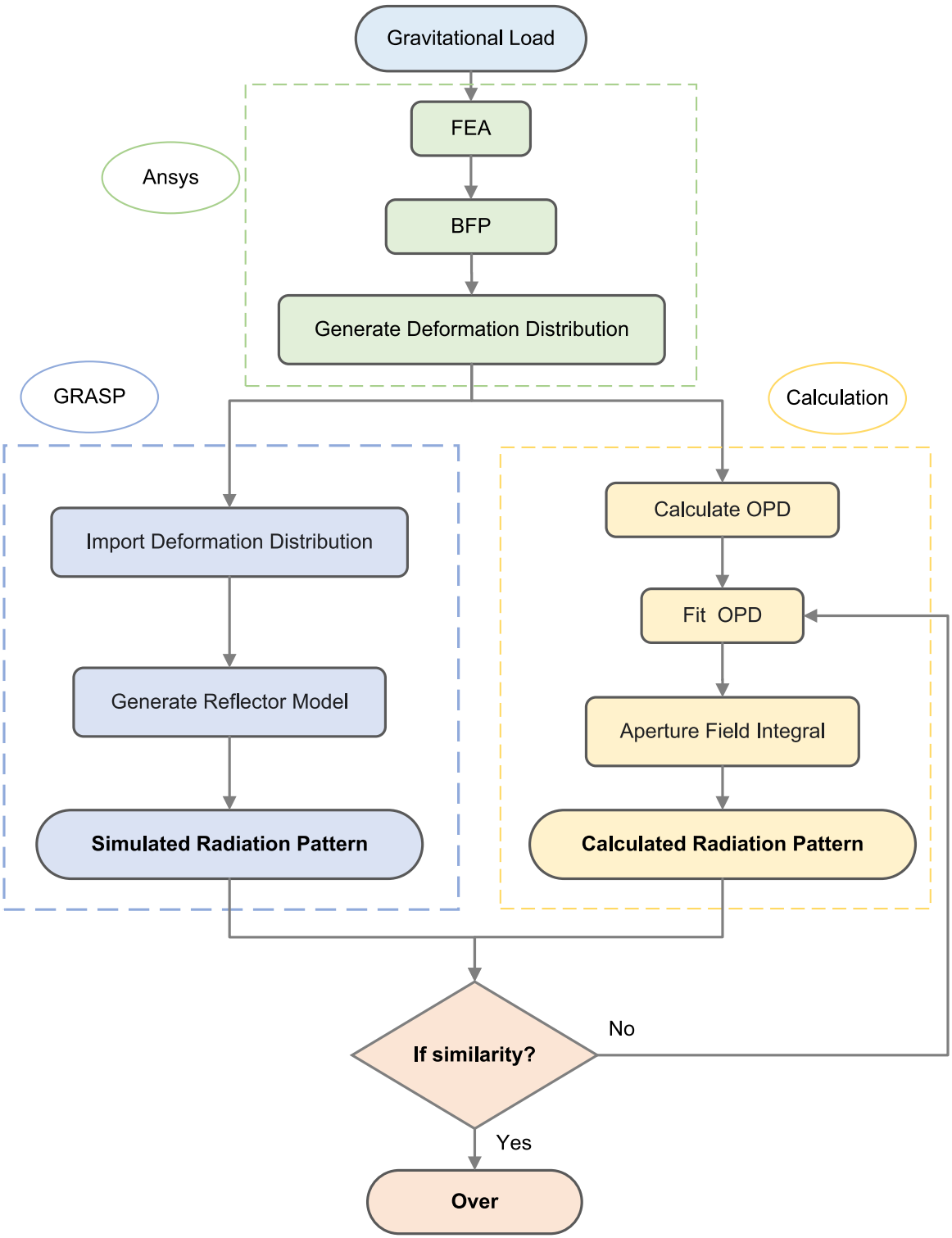

Figure 1. Schematic overview of the research methodology.

The deformation of the primary reflector due to gravitational load can be divided into two parts: the first part represents the overall rotation and translation of the paraboloid, including change in focal length, and the second part indicates the difference between the deformed surface and the fitted paraboloid. According to Ban et al. (2017), the second part is

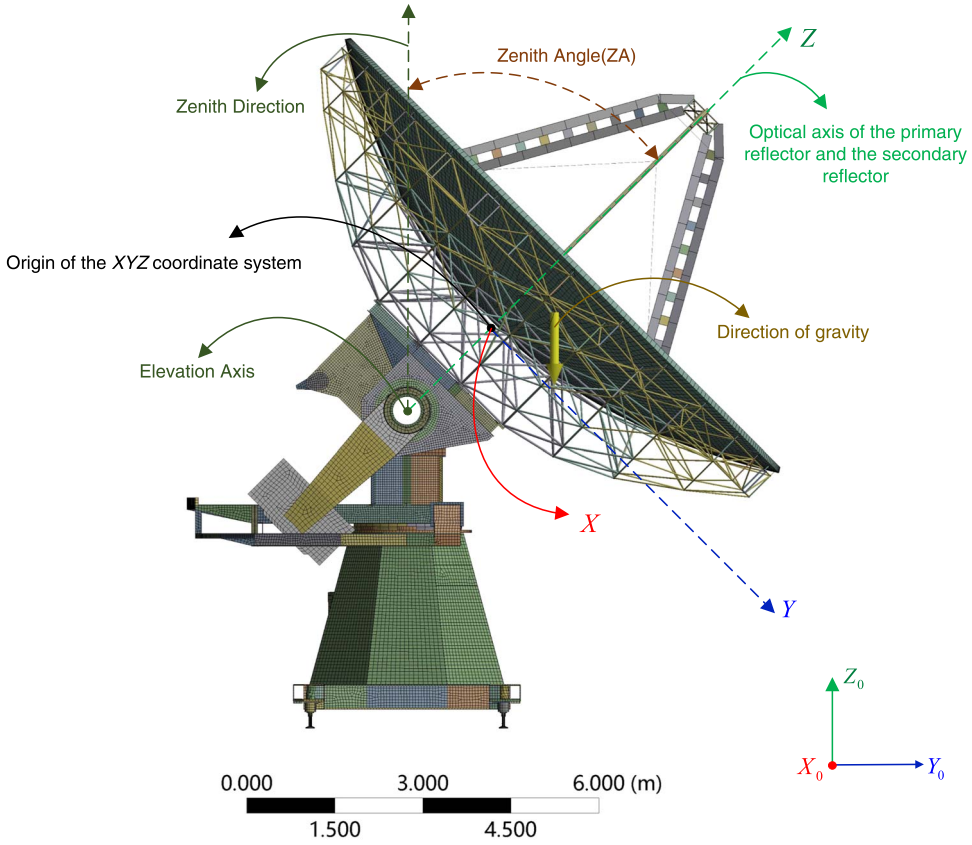

Figure 2. The FE model of the CSO telescope in Ansys.

more worthy of study. To obtain an accurate measurement of the deformation of the primary reflector, it is necessary to compute the BFP of the deformed primary reflector, and then the deformation distribution of the primary reflector can be measured by the axial error between the deformed surface and the BFP. The BFP can be fitted based on the group of data capturing the displacement of the nodes in the FE model of the primary reflector, as depicted in Figure 4.

Six parameters are employed to capture the shape and position of the BFP: d_x, d_y, d_z, d_f, ϕ_x, ϕ_y, where d_x, d_y, d_z denote the offsets of the vertex of the BFP from the vertex of the ideal paraboloid; ϕ_x,ϕ_y represent the rotation angles of the focal axis of the BFP around the *X*-axis and *Y*-axis, respectively; and d_f expresses the change in focal length.

Figure 4 shows the ideal paraboloid coordinate system and the BFP coordinate system, where the ideal paraboloid coordinate system is the antenna coordinate system (i.e., the *XYZ*-coordinate system) defined in Figure 2. The ideal paraboloid equation and the BFP equation in the *XYZ*-coordinate system can be expressed as Equations (1) and (2) respectively:

$$z = \frac{x^2 + y^2}{4f}, \tag{1}$$

$$z = \frac{(x - d_x)^2 + (y - d_y)^2}{4(f + d_f)} + d_z + y\phi_x - x\phi_y, \tag{2}$$

where f is the focal length; in most of the literatures, the *XYZ*-coordinate system is adopted as the reference coordinate system for calculating the surface errors (Fu et al. 2022; Zhang et al. 2023).

The BFP coordinate system (denoted by the *UVW*-coordinate system) in Figure 4 is used to calculate the OPD and simulate the radiation pattern. It is constructed by rotating the *XYZ*-coordinate system around the *X*-axis by the angle ϕ_x and around the *Y*-axis by the angle ϕ_y, and translating the *XYZ*-coordinate system by the distances d_x, d_y and d_z, where ϕ_x, ϕ_y, d_x, d_y, d_z are depicted in Figure 4. The least squares method is usually employed to optimize the six parameters d_x, d_y, d_z, d_f, ϕ_x, ϕ_y such that the axial error between the BFP and the deformed surface in the *UVW*-coordinate system can be minimized.

The coordinates of the nodes on the deformed surface in the *UVW*-coordinate system can be expressed by

$$(x_r, y_r, z_r) = (x'_Q, y'_Q, z'_Q)R_xR_y - (d_x, d_y, d_z), \tag{3}$$

where (x_r, y_r, z_r) represents the coordinate of the node Q' on the deformed primary reflector in the *UVW*-coordinate system, and (x'_Q, y'_Q, z'_Q) represents the coordinate of the node Q' on the

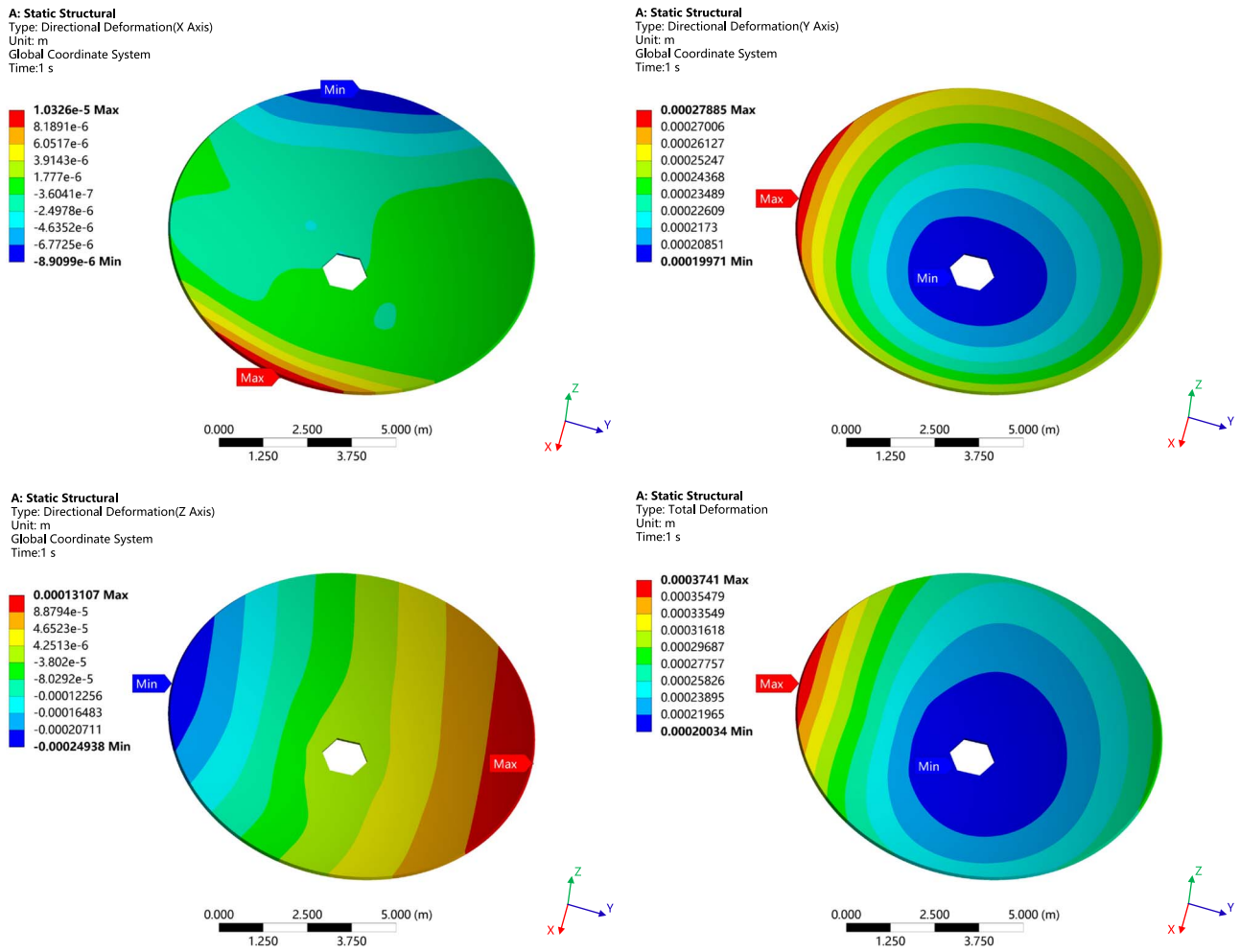

Figure 3. The deformation distribution of the primary reflector in different directions under gravitational load at ZA = 45°.

deformed primary reflector in the *XYZ*-coordinate system. The rotation matrices of the *UVW*-coordinate system with respect to the *XYZ*-coordinate system around the *X*-axis and *Y*-axis are as follows:

$$R_x = \begin{bmatrix} 1 & 0 & 0 \\ 0 & \cos\phi_x & -\sin\phi_x \\ 0 & \sin\phi_x & \cos\phi_x \end{bmatrix}, R_y = \begin{bmatrix} \cos\phi_y & 0 & \sin\phi_y \\ 0 & 1 & 0 \\ -\sin\phi_y & 0 & \cos\phi_y \end{bmatrix}.$$

Let $Q_r = (x_r, y_r, z_r')$ represent the intersection point of the BFP and a straight line going through Q' and parallel to the *W*-axis. Then the *W*-axis coordinates Z_r' of the node Q_r can be given by

$$z_r' = \frac{x_r^2 + y_r^2}{4(f + d_f)}. \quad (4)$$

To obtain the BFP of the deformed surface, the sum of squares of the axial errors between the BFP and the deformed surface in the *UVW*-coordinate system, which is defined as Equation (5), can be minimized by the least squares method.

$$T_w = \sum_{i=1}^{N} (z_{ir}' - z_{ir})^2. \quad (5)$$

Figure 5 depicts some angles and normalized radius for capturing the radiation pattern of the antenna, which is based on the BFP coordinate system (i.e., the *UVW*-coordinate system in Figure 4). φ captures the angle between the *UW* plane and a plane perpendicular to the aperture plane (i.e., the *UV*-plane) and rotating around the *W*-axis, which cuts the radiation pattern in a 3D space. If this radiation pattern-cutting plane rotates counterclockwise around the *W*-axis and starting from the positive direction of the *U*-axis, the value of φ varies from 0 to 2π. In the radiation pattern-cutting plane, θ captures the angle deviating from the positive direction of the *W*-axis, and takes the value from 0 to π (clockwise) or from 0 to $-\pi$ (counterclockwise). The angular χ represents the azimuthal aperture coordinate and r represents the normalized aperture

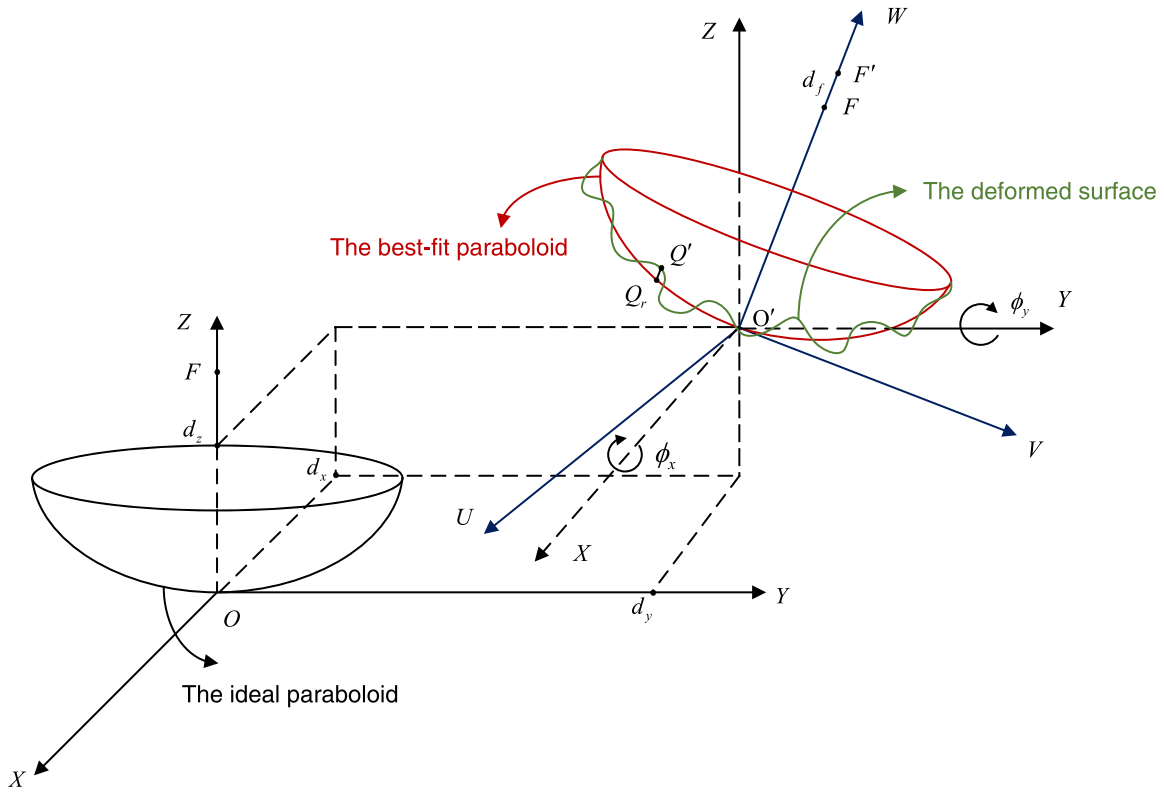

Figure 4. The relationship between the three surfaces (the ideal paraboloid, the deformed surface and the BFP).

radius in the aperture plane of the antenna. χ takes the value from 0 to 2π counterclockwise starting from the positive direction of the *U*-axis.

To analyze the radiation pattern of the deformed primary reflector, we import the data of the deformed primary reflector in the *UVW*-coordinate system to GRASP, then conduct the simulation at ZA = 45° and a frequency of 200 GHz to obtain the radiation patterns for different φs (from 0° to 180°, incremented by 1°) in the *UVW*-coordinate system (see Figure 5). In this way, we can approximately identify the values of φ and θ corresponding to the peak (i.e., the maximum gain) of the overall main lobe, which captures the deviation of the main lobe from the *W*-axis and can be defined as the pointing error. The simulation result shows that the peak of the main lobe of the radiation pattern occurs at $\varphi = 165°$ and $\theta = -0\farcs0576$, which indicates that the pointing of the deformed primary reflector's radiation pattern in the *UVW*-coordinate system is very close to the *W*-axis.

3.2. Approximate Calculation of the OPD

After determining the BFP parameters, the coordinates of the nodes on the deformed primary reflector in the *UVW*-coordinate system can be obtained by Equation (3), and the OPD in the *UVW*-coordinate system should be calculated by comparing optical path length before and after the deformation of the primary reflector and the displacement of the secondary reflector, which is depicted in Figure 6.

Assuming that the optical axis of the displaced secondary reflector is always parallel to the *W*-axis, δ_L is the lateral displacement of the secondary reflector; it may move in any direction parallel to the *UV* plane, which can be decomposed as δ_{LU} (the lateral displacement along *U*-axis) and δ_{LV} (the lateral displacement along *V*-axis), and δ_A represents the axial displacement of the secondary reflector parallel to *W*-axis. The ideal secondary reflector equation and the displaced secondary reflector equation in the *UVW*-coordinate system can be expressed as Equations (6) and (7) respectively.

$$\frac{(z - f - d_f + \sqrt{a^2 + b^2})^2}{a^2} - \frac{x^2 + y^2}{b^2} = 1, \tag{6}$$

$$\frac{(z - f - d_f + \sqrt{a^2 + b^2} - \delta_A)^2}{a^2} - \frac{(x - \delta_{LU})^2}{b^2} - \frac{(y - \delta_{LV})^2}{b^2} = 1, \tag{7}$$

where a and b represent the lengths of the major axis and minor axis of the secondary reflector respectively, f denotes the focal length and d_f expresses the change in focal length. In

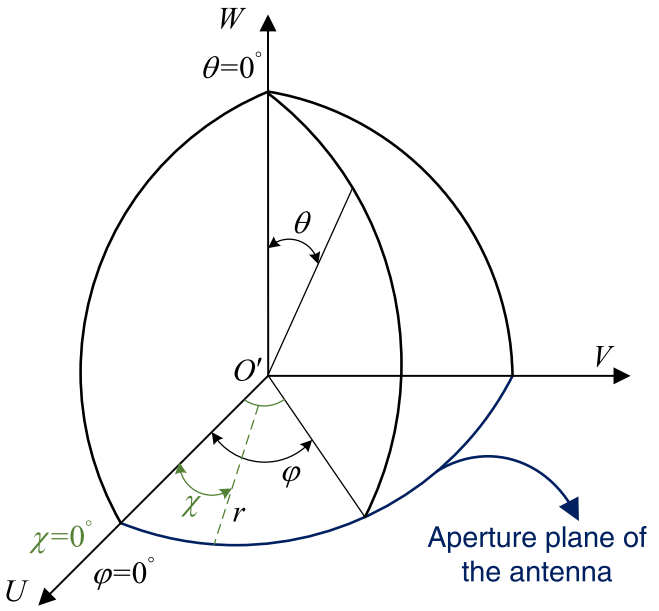

Figure 5. Description of the angles and normalized radius in the radiation pattern and the aperture plane of the antenna.

the *UVW*-coordinate system, let $S_i'(i = 1,\ldots, N)$ signify a node on the deformed primary reflector, where N is the number of nodes on the deformed primary reflector. Let F' represent the coordinate of the focal point of BFP and the ideal secondary reflector, and F'' represent the coordinate of the displaced secondary reflector. The parallel incident light from infinitely far away arrives at S_i' on the surface of the deformed primary reflector, then the light will be reflected and arrive at M_i' on the surface of the displaced secondary reflector, and finally reach F_e (i.e., the feed). S_i is the intersection point of $S_i'M_i'$ and the BFP, M_i is the intersection point of the incident light and the surface of the ideal secondary reflector, and M_iF_e is the reflected ray.

The coordinate of the point M_i' can be calculated by the coordinates of the points S_i' and F_e according to the law of light reflection, and the coordinate of point M_i can be obtained in the same way. However, numerical experimentation shows that exact calculation of the accurate coordinates of all the points M_i and $M_i'(i = 1,\ldots, N)$ is very time consuming. To improve computational efficiency, we propose an approximate method for calculating the coordinate of the point M_i' instead of the exact numerical solutions by assuming that (1) there exists a ray of light emitted from the point S_i' to the point F'', and the point M_i' will be the intersection point of the incident light $S_i'F''$ and the surface of the displaced secondary reflector; and (2) the ray of light reflected from the point M_i' will eventually reach the point F_e (M_i is calculated in the same way). Comparison study shows that the OPDs obtained by the two methods are very similar for different deformations of the primary reflector and different displacements of the secondary reflector. P_i represents the intersection point of the BFP aperture plane and a straight line going through S_i and parallel to the W-axis. P_i' signifies the intersection point of the BFP aperture plane and a straight line going through S_i' and parallel to the W-axis. Then the OPD of the node S_i' can be calculated by

$$\begin{aligned}\epsilon_i = &|M_i'F_e| + |M_i'S_i'| + |S_i'P_i'| \\ &- (|M_iF_e| + |M_iS_i| + |S_iP_i|),\end{aligned} \tag{8}$$

where ϵ_i represents the optical path length deviation due to the deformation of primary reflector surface and the displacement of the secondary reflector.

3.3. OPD Fitting Function

Since the Zernike polynomial expansion is a very efficient method to describe the general shape of the reflector surface and the optical aberrations, we adopt the first ten Zernike polynomial terms shown in Table 1 to fit the OPD distribution under the deformation of the primary reflector and the displacement of the secondary reflector. The mathematical formulation based on the Zernike polynomials in Table 1 that capture the OPD distribution over the aperture plane is given by

$$\begin{aligned}\varepsilon(r, \chi) = &(m_1 + m_2 r\cos\chi + m_3 r\sin\chi \\ &+ m_4(2r^2 - 1) + m_5 r^2\sin 2\chi + m_6 r^2\cos 2\chi \\ &+ m_7(3r^3 - 2r)\sin\chi + m_8(3r^3 - 2r)\cos\chi \\ &+ m_9 r^3\sin 3\chi + m_{10} r^3\cos 3\chi),\end{aligned} \tag{9}$$

where $m_1 - m_{10}$ are the fitting parameters that can be obtained by the least squares method, $\varepsilon(r, \chi)$ represents the OPD distribution over the aperture plane of the deformed primary reflector, χ denotes the azimuthal aperture coordinates on the aperture plane based on the *UVW*-coordinate system in Figure 5 and r signifies the normalized aperture radius.

3.4. Aperture Field Integration Method

The deformation and displacement of the reflector will cause a variation in the optical path length and thus influence the phase difference of radiation over the aperture plane, finally resulting in an interference effect leading to variations in intensity and directionality of the radiation pattern.

The AFIM is a numerical technique used to calculate the diffraction pattern or electromagnetic field distribution of a physical aperture (Yaghjian 1984). In the AFIM, the fields reflected by the primary reflector are estimated by geometrical optics rays. The reflected rays from the primary reflector are directed onto a theoretically infinite plane referred to as the aperture plane of the antenna. Conventionally, the aperture plane is considered to pass through the focal point of the paraboloid. In this paper, the AFIM is adopted to calculate the radiation pattern.

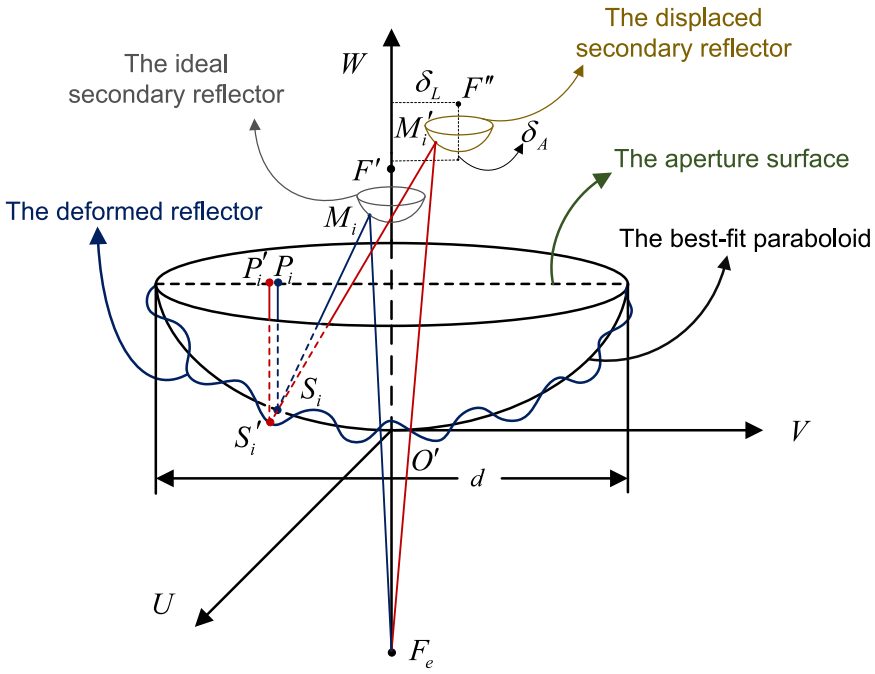

Figure 6. Illustration of the OPD's approximate calculation.

According to Baars (2007), the field intensity of radiation can be expressed by

$$E(\theta, \varphi) = \int_{r_0}^{1} \int_{0}^{2\pi} F(r, \chi) \exp\times \left[-ik\frac{dr}{2}\sin\theta\cos(\chi - \varphi)\right] r dr d\chi, \quad (10)$$

where θ, φ, χ, r are defined based on the *UVW*-coordinate system in Figure 5, $i = \sqrt{-1}$, d is the diameter and r_0 is the normalized radius of the center hole of the primary reflector. Since there is a center hole in the primary reflector of the CSO telescope, the radius of the hole is about 0.575 m, and the radius of the primary reflector is $10.4/2 = 5.2$ m, so the normalized radius of the hole is $0.575/5.2 \approx 0.1106$, therefore $r \in [0.1106, 1]$. $F(r, \chi) = A(r, \chi)\exp[i\Phi(r, \chi)]$ is the illumination function over the aperture, which consists of the amplitude function $A(r, \chi)$ and the phase function $\Phi(r, \chi)$. When there is no deformation or displacement, the phase function is usually a constant and can be omitted in the integration. In this case, the illumination function will be $F(r, \chi) = A(r, \chi)$.

In general, it is widely accepted that deformation of the primary reflector under gravitational load and small size displacement (e.g., less than one wavelength) of the secondary reflector will not affect the amplitude of the illumination function over the aperture, but will affect the phase of the illumination function (Baars 2007). Therefore, this paper concentrates on the study of the phase distribution of the aperture field caused by the deformation of the primary reflector and the small size displacement of the secondary reflector.

Table 1
The Zernike Polynomial Terms Adopted to fit the OPD

Zernike Polynomial Term	Classical Name
1	Piston
$r\cos\chi$	Tip
$r\sin\chi$	Tilt
$(2r^2 - 1)$	Defocus
$r^2\sin 2\chi$	Astigmatism
$r^2\cos 2\chi$	Astigmatism
$(3r^3 - 2r)\sin\chi$	Coma
$(3r^3 - 2r)\cos\chi$	Coma
$r^3\sin 3\chi$	Trefoil
$r^3\cos 3\chi$	Trefoil

To be consistent with the illumination function used in GRASP, the amplitude function expressed by the Gaussian distribution with an edge taper T (in dB) in this paper is given by

$$A(r, \chi) = A(r) = \exp(-\eta r^2), \quad (11)$$

where $\eta = T/20(\ln 10)$ and r is the normalized aperture radius.

When the reflector is suffering from gravitational load, the deformation of the primary reflector and the displacement of the secondary reflector will cause large-scale, systematic phase errors of radiation over the aperture plane. In this situation, the

field-pattern integral formula can be expressed by

$$E(\theta, \varphi) = \int_{r_0}^{1}\int_{0}^{2\pi} A(r, \chi)\exp(i\Delta\Phi(r, \chi)) \exp\times\left[-ik\frac{dr}{2}\sin\theta\cos(\chi - \varphi)\right]rdrd\chi, \quad (12)$$

where the phase difference function $\Delta\Phi(r, \chi)$ represents the aperture phase difference and can be expressed by the OPD function as follows

$$\Delta\Phi(r, \chi) = \frac{2\pi}{\lambda}\varepsilon(r, \chi). \quad (13)$$

4. Dual Reflectors Model in GRASP

To verify the proposed quick calculation method for radiation pattern, we construct a dual reflector model for the CSO telescope by using GRASP. The model incorporates the deformation distribution of the primary reflector and the displacement of the secondary reflector in the reflector coordinate system. Subsequently, we conduct numerical simulations to analyze the radiation pattern of the CSO telescope and compare it with the radiation pattern obtained by the quick calculation method proposed in Section 3.

GRASP@TICRA is software that is used to design and analyze general reflector antennas, and it has been identified as the electromagnetic simulation software with the highest precision and speed in the domain of reflector surface antenna computation. Figure 7 describes the model of the CSO telescope's antenna in GRASP, including the primary reflector, the secondary reflector and the feed. The detailed parameter settings of the antenna are listed in Table 2.

The dual reflector model is constructed in GRASP based on the reflector coordinate system, with the feed positioned precisely at the focal point of the secondary reflector without any displacement. Additionally, Figure 7 demonstrates the lateral displacement of the secondary reflector along the U-axis, with $\delta_{LU} = 150\ \mu$m. The primary reflector model is created by using the coordinate data of the deformed reflector in the reflector coordinate system, which is exported from Ansys, and the focal length of the primary reflector will change from f to $f + d_f$ according to the BFP parameters. The simulation of the antenna was conducted using a combination of PO and PTD.

5. Numerical Experiments and Discussion

In this section, the accuracy of the radiation pattern obtained by using the proposed quick calculation method will be verified. The verification will be conducted based on parameters and the FE model of the CSO telescope by comparing its radiation patterns obtained by the proposed quick calculation method and by simulation with GRASP. Three main FOMs of the radiation pattern are the POML, the HPBW, which equals the more known full width at half maximum (FWHM) when referring to the radiation power (de Villiers & Cotton 2022), and the gain of the first side lobe (i.e., SLL).

In this paper, all the numerical experiments were performed on a PC with an Intel i7-8700 CPU and 16 GB of RAM, which is equipped with an NVIDIA GeForce GTX 1050Ti Graphics Cards.

5.1. Radiation Pattern without Deformation or Displacement

First of all, a comparison study is conducted between the quick calculation method and the simulation method for pattern radiation analysis without the deformation of the primary reflector and the displacement of the secondary reflector. Considering that the CSO telescope works in the band with wavelengths from 2 to 0.35 mm, distinct comparative experiments were performed at both low and high frequencies. In this case, the field intensity of radiation can be expressed by Equation (14).

$$E(\theta, \varphi) = \int_{r_0}^{1}\int_{0}^{2\pi} A(r) \times \exp\left[-ik\frac{dr}{2}\sin\theta\cos(\chi - \varphi)\right]rdrd\chi. \quad (14)$$

$A(r)$ adopts the form of Equation (11), the edge taper $T = 12$ dB and $\eta = 1.3816$, which is consistent with the edge taper of the antenna model in GRASP.

An illustration of the simulation and calculation of the radiation pattern of the CSO telescope, which works at frequencies of 200 GHz and 856 GHz respectively, is depicted in Figure 8. Furthermore, Table 3 demonstrates a comparison of the main FOMs of the radiation pattern.

Based on the comparison of Figure 8 and Table 3, it can be observed that the radiation pattern and the main FOM exhibit a high degree of similarity between the simulation and quick calculation methods under both low and high frequencies. The absence of deformation and displacement results in POML $= 0''$, and the difference in HPBW and SLL between the two methods decreases with the frequency increases. Therefore, the simulation of the antenna model in Figure 7 can be used to validate the precision of the radiation pattern determined by the quick calculation method.

5.2. Radiation Pattern with Deformation and Displacement

Higher precision and a longer simulation time are often required for higher working frequencies of the CSO telescope. Consequently, to evaluate the efficiency of the proposed quick calculation method for analyzing radiation patterns, we conducted the verification experiments using the highest working frequency of the CSO telescope, i.e., 856 GHz. The computational time and accuracy of the main FOMs of the radiation pattern are employed to evaluate the effectiveness of the proposed quick calculation method.

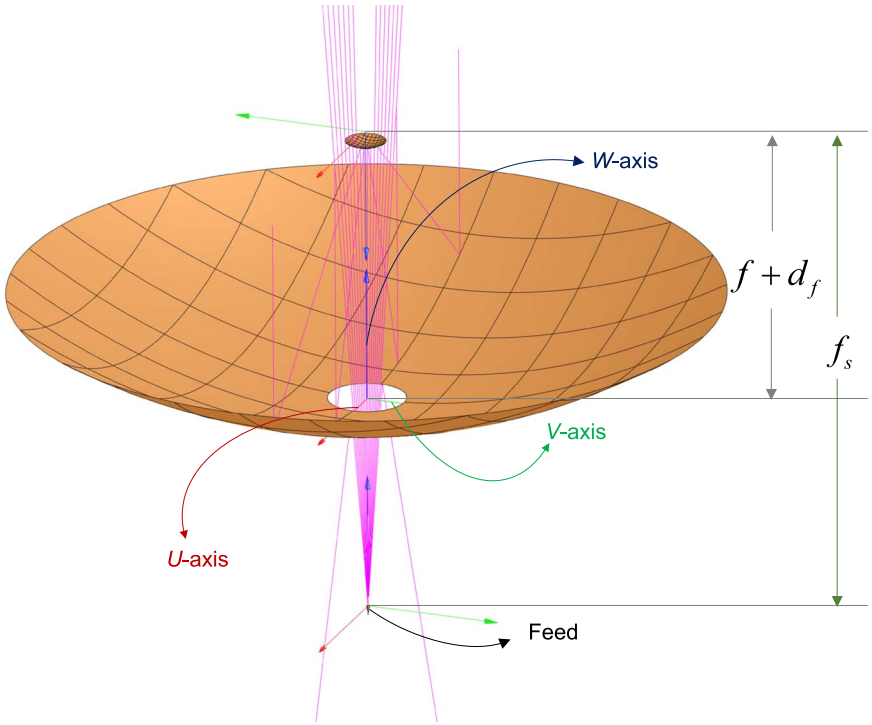

Figure 7. The model of the primary reflector and the secondary reflector of the CSO telescope in GRASP.

Table 2
Parameter Settings of the CSO Telescope's Antenna in GRASP

Primary Reflector		
Reflector diameter	d	10.4 m
Focal length	$f + d_f$	$4.123\,258 + d_f$ m
Tilt between axis	α	0°
Offset height	H	0 m
Center hole radius	r_h	0.575 m
Secondary Reflector		
Major axis	a	3.423 679 m
Minor axis	b	1.286 739 m
Eccentricity	e	1.068 294
Focal length	f_s	7.314 768 m
Reflector diameter	d_s	480 mm
Feed		
Beam pattern		Gaussian Beam
Taper level		−12 dB

First, we take the deformed primary reflector under gravitational load at ZA = 15° as an example without considering the lateral displacement of the secondary reflector. The radiation pattern under $\varphi = 0°$ calculated by the proposed method in Section 3 and simulation are presented in Figure 9, which shows that the calculated radiation pattern is very close to the simulation results in the POML and HPBW, but there is a significant difference in SLL (about 3 dB), and the shape of the side lobe is not very similar, which indicates the OPD fitting function (Equation (9)) is not precise enough on the aperture plane. Since the terms $\sin 2\chi$, $\cos 2\chi$, $\sin 3\chi$ and $\cos 3\chi$ in Equation (9) have a significant impact on the side lobe of the radiation pattern, the modification of the exponential magnitude of the aperture radius r in the four terms can affect the OPD on different aperture radii, and thus affect the shape of the side lobe and the SLL of the radiation pattern.

Therefore, we modify the exponential magnitude of the aperture radius r in the terms $r^2 \sin 2\chi$, $r^2 \cos 2\chi$, $r^3 \sin 3\chi$ and $r^3 \cos 3\chi$ in Equation (9) to a variable, and the modified OPD fitting function is as follows

$$\begin{aligned}\varepsilon(r, \chi) = (&m_1 + m_2 r\cos\chi + m_3 r\sin\chi \\ &+ m_4(2r^2 - 1) + m_5 r^{w_1}\sin 2\chi + m_6 r^{w_2}\cos 2\chi \\ &+ m_7(3r^3 - 2r)\sin\chi + m_8(3r^3 - 2r)\cos\chi \\ &+ m_9 r^{w_3}\sin 3\chi + m_{10} r^{w_4}\cos 3\chi)\end{aligned}, \tag{15}$$

where w_1, w_2, w_3 and w_4 represent the fitting parameters; we find that the side lobe ascends when w_1 and w_2 decrease and declines when w_1 and w_2 increase; when w_3 and w_4 increase, the right side lobe rises and the left side lobe falls; when w_3 and w_4 decrease, the right side lobe falls and the left side lobe rises. Through comparative experiments, we observe that when w_1, w_2, w_3 and w_4 are all small but greater than 0, the calculated

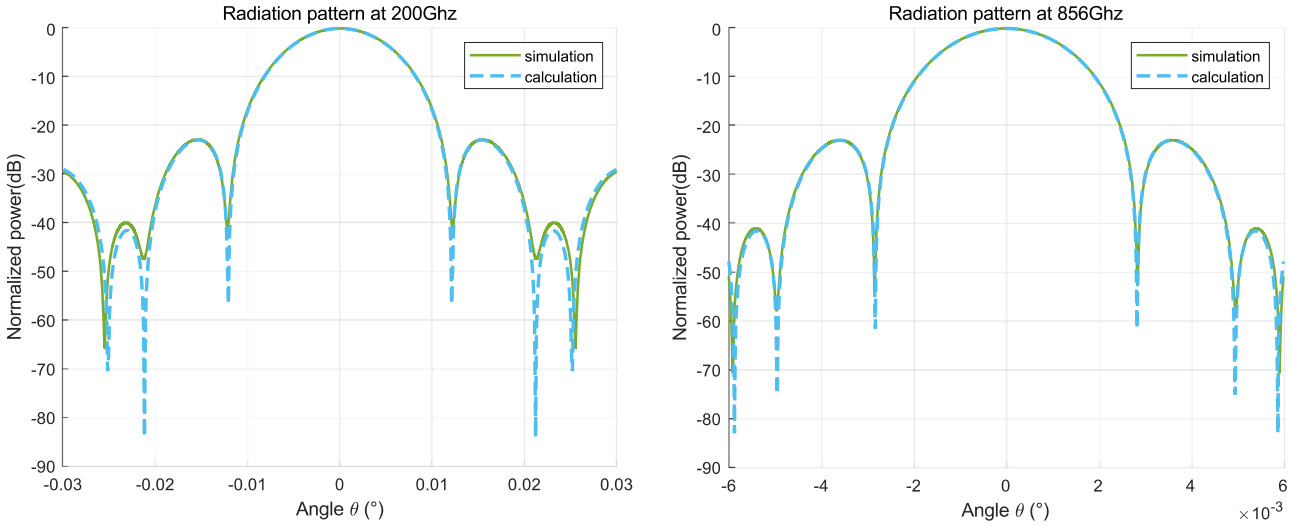

Figure 8. The radiation pattern obtained by simulation and calculation at the frequencies of 200 GHz and 856 GHz respectively.

Table 3
The FOM of the Radiation Pattern Without Deformation or Displacement

Frequency (GHz)	Method	POML (″)	HPBW (″)	SLL (dB)
200	Simulation	0	34.704	−22.8740
	Calculation	0	34.524	−22.9611
856	Simulation	0	8.100	−22.9281
	Calculation	0	8.100	−22.9612

side lobe will be closer to the simulated side lobe than using Equation (9), while the POML and HPBW remain invariant. Therefore, we limit the range of exponential magnitude of the aperture radius of r in the interval [0, 0.2], and automatically optimize the values of w_1, w_2, w_3 and w_4 by the least squares method to obtain the modified OPD fitting function, and the radiation pattern calculated by the modified OPD fitting function is shown in Figure 9. It can be seen that not only the SLL calculated by the modified OPD fitting function is more similar to the simulation results, but also the shape of the side lobe is closer to the simulated side lobe.

In order to verify the rapidity and accuracy of the proposed calculation method with the deformation of the primary reflector and the displacement of the secondary reflector, we sequentially investigate the accuracy of the modified OPD fitting function, the improvement of the calculation method in computational efficiency and the accuracy of the calculation method in obtaining the radiation pattern.

For the verification of the fitting effect of the modified OPD fitting function, we consider the gravitational deformation of the primary reflector of the CSO telescope at three typical ZAs, i.e., 0°, 45° and 75°, and simultaneously consider the case that the lateral displacement of the secondary reflector is $\delta_{LU} = 150\ \mu$m (which is almost half of the wavelength at an operating frequency of 856 GHz) and $\delta_{LV} = 0\ \mu$m, and the axial displacement of the secondary reflector is $\delta_A = 0\ \mu$m. The calculated OPD distributions according to Equation (8) at ZA = 0°, 45° and 75° are depicted in Figures 10 (a1), (b1) and (c1). Figures 10 (a2), (b2) and (c2) exhibit the OPD distribution obtained by the modified OPD fitting function (Equation (15)) for ZA = 0°, 45° and 75° respectively. The differences between the OPD distributions obtained by the two methods are depicted in Figures 10 (a3), (b3) and (c3), and the root mean squares of the differences for ZA = 0°, 45° and 75° are 8.14 μm, 12.22 μm and 14.14 μm respectively. It can be seen that the OPD distribution obtained by Equation (15) has a high similarity with that obtained by Equation (8).

In order to evaluate the rapidity of the quick calculation method for obtaining the radiation pattern at the highest working frequency (i.e., 856 GHz) of the CSO telescope, experimental analyses are systematically conducted by considering the inevitable deformation of the primary reflector under gravitational load at different ZAs varying from 0° to 75° (i.e., 0°, 15°, 30°, 45°, 60°, 75°) and the lateral displacement of the secondary reflector $\delta_{LU} = 150\ \mu$m. The property of the radiation pattern is mainly dominated by the main lobe and the first side lobe region, which can be covered by $\theta \in [-0.^\circ006, 0.^\circ006]$ (i.e., $[-21.''6, 21.''6]$) at 856 GHz. To obtain a high accuracy of the FOM, the interval of θ is taken to be $0.^\circ00001$ (i.e., $0.''036$). The time for obtaining the radiation pattern by the proposed calculation method and simulation is presented in Table 4.

The results in Table 4 show that with the increase of ZA from 0° to 75°, the time for obtaining the radiation pattern increases for both the simulation and calculation methods. For the CSO telescope with an operating frequency of 856 GHz, the average time for the proposed quick calculation method is 103.68 seconds compared to 1.23 hr for the simulation method.

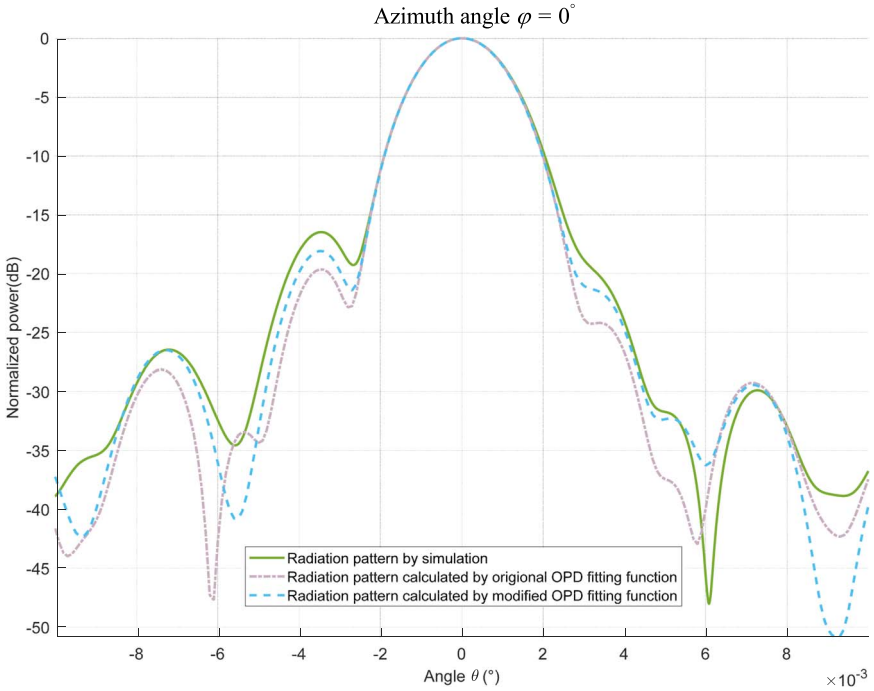

Figure 9. The radiation patterns under $\varphi = 0°$ obtained by simulation, calculated by the original OPD fitting function (Equation (9)) and calculated by the modified OPD fitting function (Equation (15) with $m_1 = -1.80 \times 10^{-7}$, $m_2 = 1.38 \times 10^{-7}$, $m_3 = 1.46 \times 10^{-5}$, $m_4 = -3.89 \times 10^{-7}$, $m_5 = -6.92 \times 10^{-6}$, $m_6 = -1.45 \times 10^{-7}$, $m_7 = 2.74 \times 10^{-6}$, $m_8 = -7.41 \times 10^{-8}$, $m_9 = -4.87 \times 10^{-7}$, $m_{10} = 8.75 \times 10^{-7}$, $w_1 = 0.0403$, $w_2 = 0.1658$, $w_3 = 0.0031$, $w_4 = 0.1729$), in the situation with the deformation of the primary reflector at ZA = 15° and without lateral displacement of the secondary reflector.

The proposed quick calculation method reduces the time significantly (by 42.7 times) for obtaining the radiation pattern compared to simulation.

To evaluate the accuracy of the radiation pattern obtained by the quick calculation method, the radiation patterns under $\varphi = 0°$, which is parallel to the displacement of the secondary reflector and obtained by simulation and quick calculation, are shown in Figure 11. The comparisons of POML, HPBW and SLL obtained by simulation and calculation in Figure 11 are displayed in Table 5.

Figure 11 shows that the calculated and simulated radiation patterns are very close to each other with the lateral displacement of the secondary reflector $\delta_{LU} = 150\ \mu$m and the primary reflector under gravitational deformation at different ZAs, and the FOMs of the radiation pattern presented in Table 5 show that the POML reduces for both simulated and calculated methods with the increase of ZA, and the maximum difference between the simulated and calculated results is less than $0\farcs036$. The HPBW becomes wider for both simulation and calculation as ZA increases, with the maximum deviation occurring at ZA = 60° and ZA = 75°, which is $0\farcs18$. Both the simulated and calculated SLL rise with increasing ZA, and the average difference is 0.9668 dB.

From the performances of the radiation pattern represented in Tables 4–5, it can be concluded that for the deformation of the primary reflector under gravitational load and a lateral displacement of the secondary reflector for about half a wavelength, the quick calculation method can significantly enhance the efficiency of calculating the radiation pattern during the structural design phase and maintain a high level of accuracy compared to simulation based on PO and PTD.

5.3. Comparison for various Displacements of the Secondary Reflector

To illustrate the general applicability of the proposed quick calculation method, we compare the similarity of the radiation pattern obtained by the quick calculation method and the simulation by considering (i) the deformation of the primary reflector of the CSO telescope under gravitational load at ZA = 15° and an operating frequency of 856 GHz, and (ii) the displacements of the secondary reflector along the U-axis from 0 to 350 μm (the wavelength at 856 GHz). The radiation patterns under $\varphi = 0°$ with different lateral displacements of the secondary reflector (i.e., 0, 50, 100, 150, 200, 250, 300, 350 μm) by simulation and quick calculation method are shown in Figure 12. The comparisons of the POML, HPBW and SLL obtained by simulation and calculation in Figure 12 are displayed in Table 6.

From Figure 12 and Table 6, it can be observed that when the lateral displacement of the secondary reflector (δ_{LU}) gradually increases from 0 to the working wavelength (i.e.,

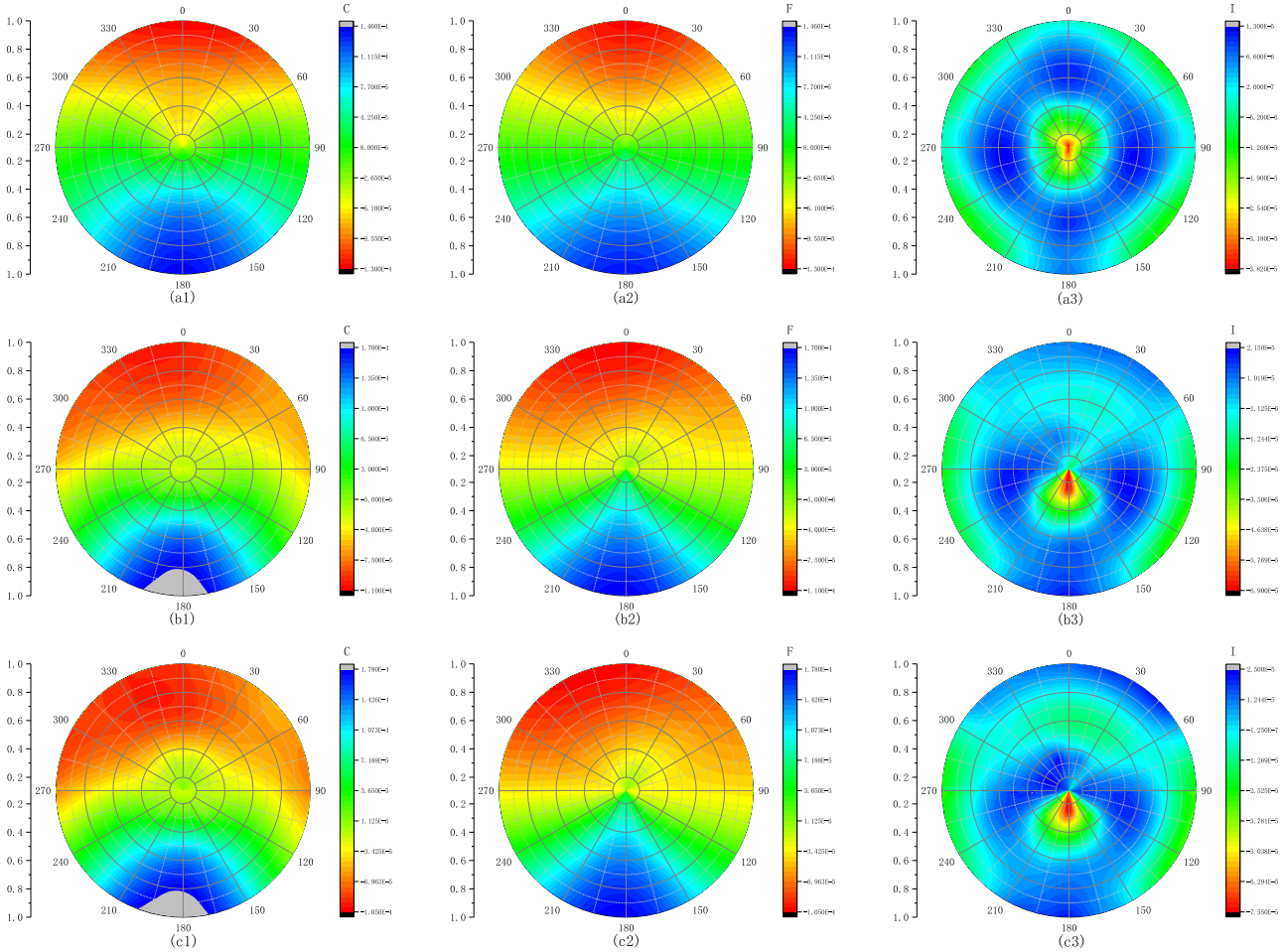

Figure 10. The distribution of the OPD on the aperture plane based on the deformed primary reflector under gravitational load and the lateral displacement of the secondary reflector $\delta_{LU} = 150$ μm (the unit is m): (a1) the OPD distribution obtained by Equation (8) at ZA = 0°; (b1) the OPD distribution obtained by Equation (8) at ZA = 45°; (c1) the OPD distribution obtained by Equation (8) at ZA = 75°; (a2) the OPD distribution obtained by Equation (15) at ZA = 0°; (b2) the OPD distribution obtained by Equation (15) at ZA = 45°; (c2) the OPD distribution obtained by Equation (15) at ZA = 75°; (a3) the difference between the OPD distributions obtained by Equations (8) and (15) at ZA = 0°; (b3) the difference between the OPD distributions obtained by Equations (8) and (15) at ZA = 45°; (c3) the difference between the OPD distributions obtained by Equations (8) and (15) at ZA = 75°.

Table 4
Time for Obtaining the Radiation Pattern by Simulation and Quick Calculation

ZA (°)	Time	
	Simulation (hr)	Calculation (s)
0	1.08	98.82
15	1.19	100.67
30	1.24	102.65
45	1.29	105.22
60	1.30	107.03
75	1.28	107.68

350 μm), the POML increases and the HPBW gets wider, and the differences of POML and HPBW between the calculation and simulation method are always less than 0.″036. As the lateral displacement of the secondary reflector increases from 0 to 100 μm (i.e., about 0.3 working wavelength), the SLL is determined by the left side lobe, and both the simulated and calculated SLLs decline, with the difference between them increasing from 1.6021 dB (for $\delta_{LU} = 0$ μm) to 2.0638 dB (for $\delta_{LU} = 100$ μm). When δ_{LU} is greater than 150 μm, the SLL is dominated by the right side lobe, and both the simulated and calculated SLLs ascend, with the difference between them decreasing from 0.6559 dB (for $\delta_{LU} = 150$ μm) to 0.1651 dB (for $\delta_{LU} = 350$ μm). The experimental results show that the shape of the calculated radiation patterns is very similar to the simulated radiation patterns not only in the main lobe region but also in the side lobe region, and the proposed quick calculation method can track the radiation pattern of the simulation more accurately with the increase of the lateral displacement of the secondary reflector.

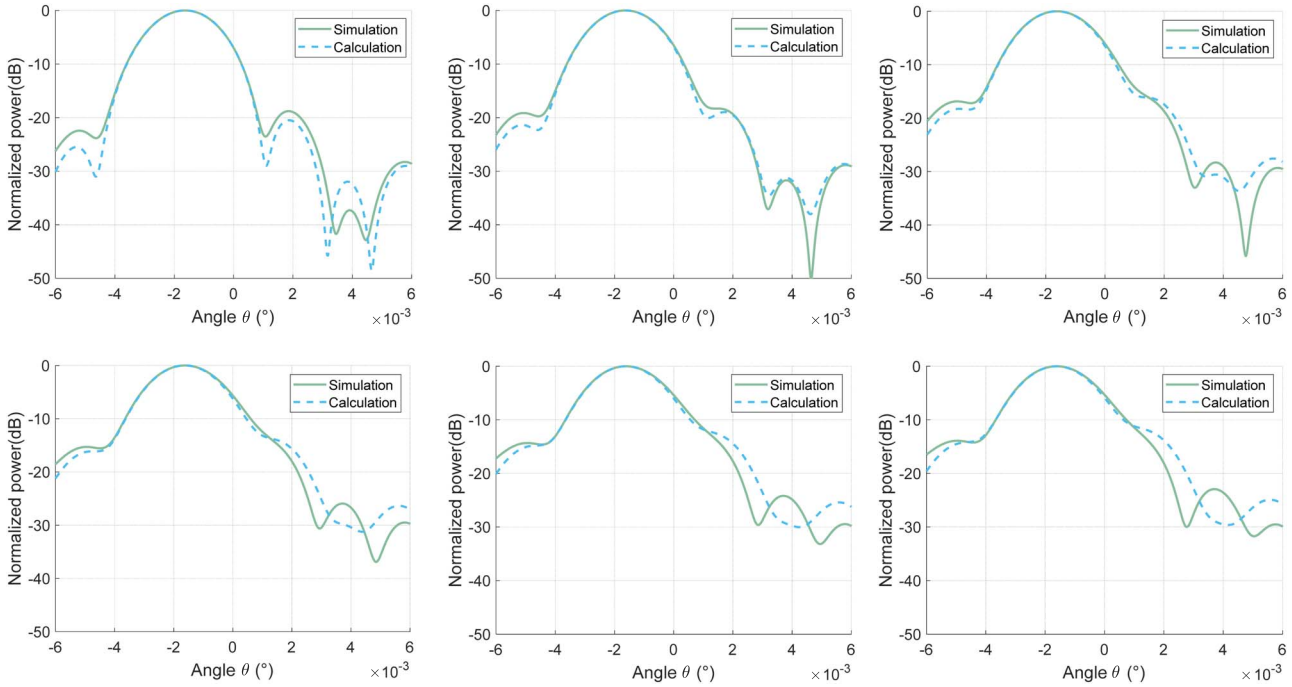

Figure 11. The radiation pattern under $\varphi = 0^\circ$ with the deformation of the primary reflector at different ZAs and a lateral displacement (δ_{LU}) of 150 μm of the secondary reflector.

Table 5
The FOMs in the Radiation Pattern Under $\varphi = 0^\circ$ with the Deformation of the Primary Reflector and a Lateral Displacement (δ_{LU}) of 150 μm of the Secondary Reflector between Simulation and Calculation

FOM	Method	ZA (°)					
		0	15	30	45	60	75
POML (″)	Simulation	−5.904	−5.868	−5.832	−5.832	−5.796	−5.796
	Calculation	−5.868	−5.868	−5.868	−5.832	−5.832	−5.832
HPBW (″)	Simulation	8.064	8.172	8.244	8.352	8.460	8.460
	Calculation	8.136	8.136	8.172	8.208	8.280	8.280
SLL (dB)	Simulation	−18.7963	−18.3103	−16.8613	−15.2938	−14.3264	−13.9017
	Calculation	−20.4900	−18.9662	−18.2613	−16.1242	−14.9882	−14.4605

6. Conclusion

The radiation pattern captures the electromagnetic properties for a radio telescope to receive radiation from target sources in the sky. It also has a significant influence on the pointing accuracy, sensitivity, and angular resolution of the telescope. For submillimeter telescopes operating at high frequencies, the deformation of the primary reflector under gravitational load and the displacement of the secondary reflector significantly affect the radiation pattern. Therefore, a quick and accurate calculation method for radiation pattern analysis is of good significance for a submillimeter telescope to improve the efficiency of radiation pattern analysis during the structural design phase.

In this paper, we propose an approximate OPD calculation method for the deformation of the primary reflector under gravitational load and the displacement of the secondary reflector, and an OPD fitting function by the modified Zernike polynomials is presented based on the calculated OPD. Then a quick calculation method for the radiation pattern of a submillimeter telescope is obtained by combining the modified OPD fitting function with the aperture field integration. Numerical experiments are conducted for the CSO telescope to verify the rapidity and accuracy of the proposed quick calculation method for obtaining the radiation pattern at the highest working frequency of 856 GHz. The experimental results show that the quick calculation method can significantly

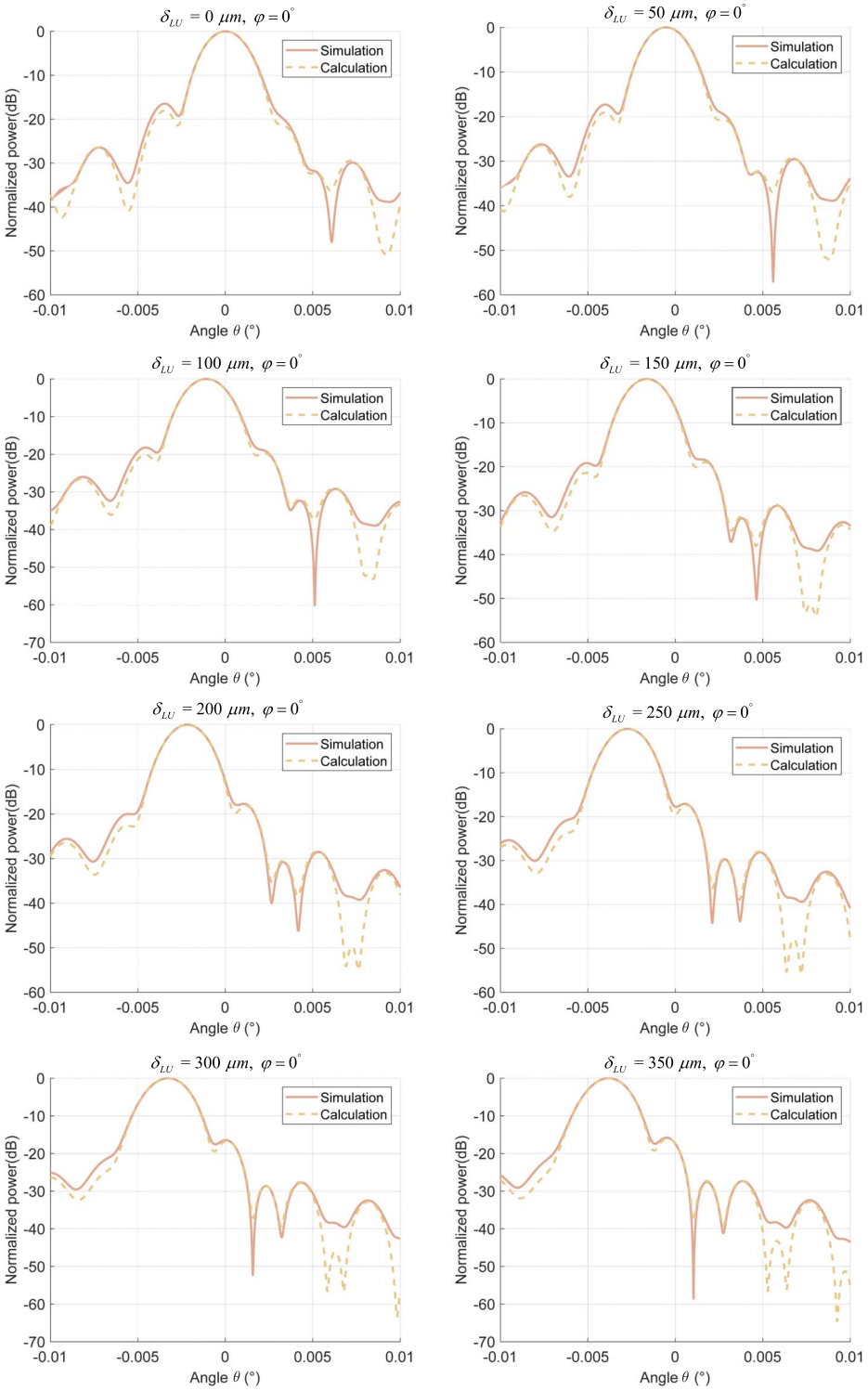

Figure 12. The radiation pattern under $\varphi = 0°$ with the deformation of the primary reflector at ZA $= 15°$ and different lateral displacements of the secondary reflector.

reduce the time to obtain the radiation pattern by 42.7 times (from 1.23 hr to 103.68 s) compared to the simulation method by PO and PTD in GRASP, which is very beneficial in the radiation pattern analysis during the optimized structural design phase. Moreover, the quick calculation method also shows high accuracy in the three main FOMs (i.e., the POML, the HPBW,

Table 6
The Difference in FOM between Simulation and Calculation Under various Lateral Displacements of the Secondary Reflector with the Deformation of the Primary Reflector Under Gravitational Load at ZA = 15° Under $\varphi = 0°$

FOM	Method	The Magnitude of the Lateral Displacement (μm) along the U-axis							
		0	50	100	150	200	250	300	350
POML (″)	Simulation	0.036	−1.944	−3.888	−5.868	−7.848	−9.792	−11.772	−13.716
	Calculation	0.000	−1.944	−3.924	−5.868	−7.812	−9.792	−11.736	−13.716
HPBW (″)	Simulation	8.136	8.136	8.136	8.172	8.172	8.208	8.208	8.244
	Calculation	8.100	8.136	8.136	8.136	8.172	8.172	8.208	8.244
SLL (dB)	Simulation	−16.4611	−17.3248	−18.2286	−18.3103	−17.7281	−17.0854	−16.4353	−15.7987
	Calculation	−18.0632	−19.0806	−20.2924	−18.9662	−18.1497	−17.3758	−16.6492	−15.9638

and the SLL) under the deformation of the primary reflector and the displacement of the secondary reflector compared to the simulation results.

The effectiveness of the quick calculation method for radiation patterns for the deformation of the primary reflector under gravitational load and the displacement of the secondary reflector has been verified in this paper. Other factors (e.g., wind force and thermal gradient) that affect the pointing accuracy will be taken into account for future research, including the method of calculating deformation distribution under these factors and the technique of compensating for the degradation of the radiation pattern due to these factors.

Acknowledgments

This research is supported by Open Fund of State Key Laboratory of Infrared Physics, Shanghai Institute of Technical Physics, Chinese Academy of Sciences.

References

Baars, J. W., & Kärcher, H. J. 2018, Radio Telescope Reflectors, Vol. 447 (Berlin: Springer)
Baars, J. W. M. 2007, The Paraboloidal Reflector Antenna in Radio Astronomy and Communication, Vol. 348 (Berlin: Springer)
Ban, Y., Duan, B., Wang, C., et al. 2017, ITAP, 65, 3392
de Villiers, M. S., & Cotton, W. D. 2022, AJ, 163, 135
Du, X., Landecker, T. L., Robishaw, T., et al. 2016, PASP, 128, 115006
Duan, B. Y., & Wang, C. S. 2009, ITAP, 57, 3409
Feng, S., Duan, B., Wang, C., Ban, Y., & Wang, W. 2019, IEEEA, 7, 140328
Fu, L. B., Liu, J. J., Yan, W., et al. 2022, RAA, 22, 095001
Li, P., Duan, B. Y., Wang, W., & Zheng, F. 2012, IAPM, 54, 40
Lian, P., Duan, B., Wang, W., Xiang, B., & Hu, N. 2015, ITAP, 63, 2312
McNamara, D. A., Pistorius, C. W. I., & Malherbe, J. A. G. 1990, Introduction to the Uniform Geometrical Theory of Diffraction (Norwood, MA: Artech House Norwood)
Rahmat-Samii, Y., & Haupt, R. 2015, IAPM, 57, 85
Safak, M. 1990, ITAP, 38, 117
Woody, D., Vail, D., & Schaal, W. 1994, Proc. IEEE, 82, 673
Xiang, B. B., Wang, C. S., Lian, P. Y., Wang, N., & Ban, Y. 2019, RAA, 19, 62
Yaghjian, A. 1984, ITAP, 32, 1355
Zhang, Z. H., Ye, Q., Fu, L., et al. 2023, RAA, 23, 015001